FULL PAPER

3D-QSAR and Molecular Docking Studies of *p*-Aminobenzoic Acid Derivatives to Explore the Features Requirements of Alzheimer Inhibitors

Khalil El Khatabi, Ilham Aanouz, Reda El-mernissi, **Ayoub Khaldan, Mohammed Aziz Ajana*, Mohammed Bouachrine, and Tahar Lakhlifi**

Molecular chemistry and Natural Substances Laboratory Faculty of Sciences. University Moulay Ismail BP 11201-Zitoune. Meknès. 50000. Morocco.

Abstract:

In search of novel and more potent p-aminobenzoic acid derivatives previously evaluated as effective acetylcholinesterase inhibitors for the control of Alzheimer's disease (AD), an integrated computational approach of three-dimensional quantitative structure–activity relationship and molecular docking were performed on a series of 20 compounds. The 3D-QSAR approach was applied to statistically study the structure-activity relationships (SAR) and had yielded good statistical significance for two high predictive models; comparative molecular field analysis (CoMFA: Q^2=0.785; R^2=0.936; $rext^2$= 0.818) and comparative molecular similarity indices analysis (CoMSIA: Q^2=0.831; R^2=0.944; $rext^2$= 0.931). Detailed analysis of the predictive models contour maps revealed that the hydrophobic and electrostatic fields govern the bioactivity and provided much helpful information to understand the features requirement in order to develop new potent acetylcholinesterase inhibitors. These findings were very useful for designing four novel inhibitors with enhanced activities targeting acetylcholinesterase. Through molecular docking, the newly designed compounds and compound 19 were docked on AChE as the protein target which helped to analyze the interaction characteristics and explore the binding modes at the active sites of the AChE. This work may be of utility for guiding the rational design of a new generation of acetylcholinesterase inhibitors.

Keywords: 3D-QSAR; acetylcholinesterase activity; molecular docking; molecular modeling; *p*-aminobenzoic acid

1. Introduction

Alzheimer's disease (AD) is the most widespread reason of all neurodegenerative. It is a chronic progressive neurodegenerative disorder and adversely affecting the cognitive processes and intellectual capabilities [1, 2]. AD is a creating alarming situation and an increasing issue across all nations, mostly affecting the older population [3]. The characteristically symptoms of Alzheimer's disease are characterized by cognitive dysfunction including loss of reasoning skills, disorientation, increased apathy, delusions, troubles with language, and other delicate troubles in the executive cognitive functions along with physical disability, which would be difficult enough to perform daily life activities [4], [5]. Although the exact cause of AD remains unclear, many pathogenic mechanisms including metabolic, genetic, environmental factors, and lifestyle are suggested to be involved in the appearance and progression of the disease [6]. The AD is associated with deficits in cholinergic neurotransmission [7], bio metals dysfunction [8, 9], formation of toxic β-amyloid (Aβ) plaques [10], inflammation and increased oxidative stress [11], destabilization of calcium homeostasis [12] and neurofibrillary tangles [13].

Acetylcholine (Ach) is a crucial neurotransmitter for the cognitive function, so that

---

*Corresponding author. E-mail: ✉ a.ajanamohammed@fs.umi.ac.ma

the first line of treatment is to increase the acetylcholine levels at synapses [14]. The plurality of cholinergic signaling problems is treated by acetylcholinesterase inhibitors. Acetylcholinesterase is able to parry the hydrolysis of Acetylcholine, leading to the reduction of synaptic availability of that substance in the brain. Consequently, the research for anti-AD therapeutic agents is based on the restoration of the acetylcholine level in the synaptic cleft achieved by acetylcholinesterase inhibition [15]. Shrivastava and *al.* [16] have designed and synthesized some p-aminobenzoic acid (PABA) derivatives and evaluated against acetylcholinesterase for the management of AD. p-aminobenzoic acid is an amino acid compound and its derivatives are endowed with extensive biological activities [17]. The drugs containing PABA scaffold are considered well-tolerated and non-toxic [18]. The PABA structure moiety has recently featured as an important pharmacophore for the cholinesterase inhibition. For this reason, the design and development of alternative PABA candidates for the control of cholinesterase levels is essential for the treatment of AD.

The current study aimed to guide the rational design of new acetylcholinesterase inhibitors with more efficiency for the control of AD using reliable approaches such as 3D-QSAR and molecular docking. Therefore, 20 p-aminobenzoic acid derivatives were selected to build reliable and robust CoMFA and CoMSIA-3D-QSAR models.

Thereafter, by analyzing the contour maps of the optimal models, four new PABA derivatives possessing improved binding affinity were proposed, and molecular docking was then explored to evaluate the structural stability of the newly designed compounds at the active site of acetylcholinesterase.

2. Results and Discussion

2.1 Statistical analysis and validation

2.1.1 CoMFA and CoMSIA

CoMFA model was associated with a remarkably high Q2 of 0.785, R2 of 0.936, F-test value F of 87.84, and 0.319 as standard error of estimate for two optimum components. The proportions of steric and electrostatic contributions were at 80.4% and 19.6%, respectively. The Q2, R2, F, SCV and N values obtained from the CoMSIA were 0.831, 0.944, 100.5, 0.229 and 2, respectively. The proportions of steric, electrostatic, H-bond acceptor, H-bond donor and hydrophobic contributions accounted for 15.5%, 24.9%, 0.083%, 15.6%, and 35.8%, respectively. The external validation correlation coefficient rext2 values of 0.818 for CoMFA and 0.931 for CoMSIA, indicating good reliability of the models using five molecules as test set. The detailed PLS results are summarized in Table 1. The Experimental and predicted pIC50 of the optimal models are shown in Table 2.

Table 1. Summary of PLS results.

Model	Q^2	R^2	S_{CV}	F	N	r_{ext}^2	Fractions				
							Ster	Elect	Acc	Don	Hyd
CoMFA	0.785	0.936	0.319	87.84	2	0.818	0.804	0.196	-	-	-
CoMSIA	0.831	0.944	0.229	100.5	2	0.931	0.155	0.249	0.083	0.156	0.358

R^2: Non-cross-validated correlation coefficient; Q^2: Cross-validated correlation coefficient; r_{ext}^2: External validation correlation coefficient; S_{cv}: Standard error of the estimate; N: Optimum number of components; F: F-test value.

2.2 Contour map analysis

To identify the key features contributing to the binding affinity of the compounds, CoMFA and CoMSIA contour maps were generated as displayed in Figures 1 and 2 respectively. The most active compound 19 of the database was used as a representative molecule.

2.2.1 CoMFA Contour Maps

As depicted in Figure1-A, the green contours (80% contribution) indicate sterically favorable bulky substituents, whereas yellow parts (20% contribution) depict areas where less bulky groups would be beneficial for activity. A yellow contour was distributed around position 4 of the phenyl moiety over the hydroxyl group, indicating the insignificance of steric bulky groups at this position. For example, compounds 18 and 19 showed higher AChE inhibitor activities than that

173

Orbital: Electron. J. Chem. 12 (4): 172-181, 2020

of compounds 10 and 11. The green region indicated that the incorporation of steric bulky substituent in the position 4 of the phenyl moiety at R1 would be favorable for the potency, which could be demonstrated by compounds 18 and 19.

The red (20% contribution) and blue (80% contribution) contours (Fig. 1-B) represent the positions where electronegative charge groups and electropositive charge groups would be favorable to achieve high inhibitory activity,

respectively. A medium-sized blue contour is observed near the position 4 of the phenyl ring, representing the importance of electropositive groups in this position, another one could be found near the acid group, meaning that introducing positively charged substituents in this region would be favorable. There are two red quadrilaterals near the position 5 of the phenyl moiety at R2 from both sides, indicating that electronegative groups at these areas would exhibit good anti-Alzheimer activity.

Table 2. Experimental and predicted pIC50 of PABA derivatives.

| N°	pIC50	CoMFA		CoMSIA	
		predicted	Residuals	predicted	Residuals
1	4.372	4.894	-0.522	4.904	-0.532
2	4.991	4.991	0	4.900	0.001
3	5.670	5.114	0.566	5.054	0.626
4	4.686	5.000	-0.314	4.961	-0.275
5	4.188	4.348	-0.160	4.403	-0.215
6	4.049	4.135	-0.086	4.132	-0.083
7	3.941	3.937	0.005	3.963	-0.022
8*	3.965	3.634	0.331	3.627	0.324
9*	6.900	6.279	0.621	6.305	0.595
10	5.079	4.965	0.104	4.972	0.111
11	5.124	4.652	0.472	4.656	0.476
12	5.327	5.177	0.150	5.159	0.168
13	4.544	4.877	-0.333	4.870	-0.326
14	4.663	4.501	0.162	4.514	0.149
15	7.301	7.497	-0.196	6.990	0.311
16*	5.190	5.401	-0.211	5.437	-0.247
17*	4.801	5.116	-0.315	5.123	-0.322
18	7.301	7.497	-0.196	7.473	-0.172
19	7.337	7.426	-0.089	7.443	-0.106
20*	5.078	5.512	-0.432	5.448	-0.370

* Test set molecules.
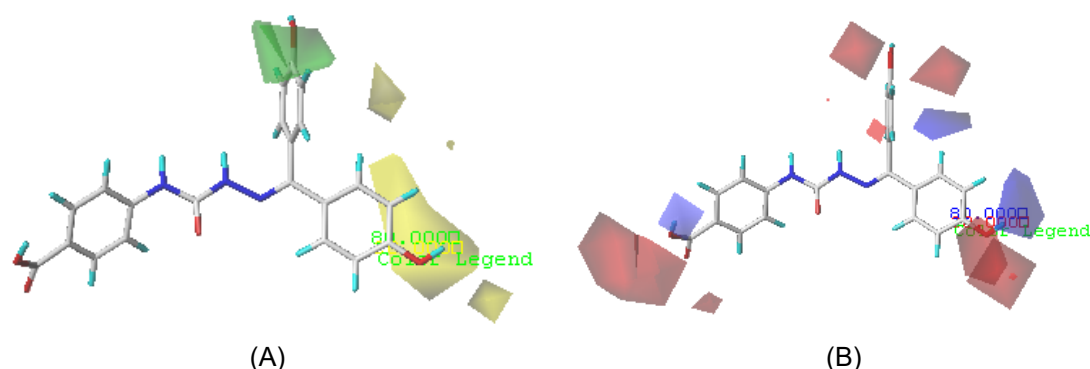
Figure 1. CoMFA contour maps for compound 19. **A)** Steric fields. **B)** Electrostatic fields.

2.2.2 CoMSIA Contour Map

CoMSIA steric and electrostatic contour maps displayed in (Fig. 2-A and 2-B) showed similar results as CoMFA (Fig. 1-A and 1-B) in almost all

174

Orbital: Electron. J. Chem. 12 (4): 172-181, 2020

aspects. Hence, analysis for these two contour maps would agree well with the CoMFA contour maps analysis.

The proportion of H-bond acceptor (HA) contribution in CoMSIA model is at 8.3% which indicates that it is not the most influencing factor to the inhibitory activity.

In the map of the hydrophobic field (Fig. 2-C), the white color (20% contribution) indicate that hydrophilic groups are favored for improving the bioactivity, while the yellow color (80% contribution) depicts an increase in the bioactivity of the hydrophobic substituents. A medium-sized yellow contour could be observed near the position 5 of the phenyl moiety at R1, which designates that the addition of hydrophobic substituents near these yellow areas might increase the inhibitory activity. In addition, two medium-sized white contours were observed around the position 4 of the phenyl moiety of R2 and almost all positions of R1 indicate that hydrophilic group substitution near the white regions could increase the activity.
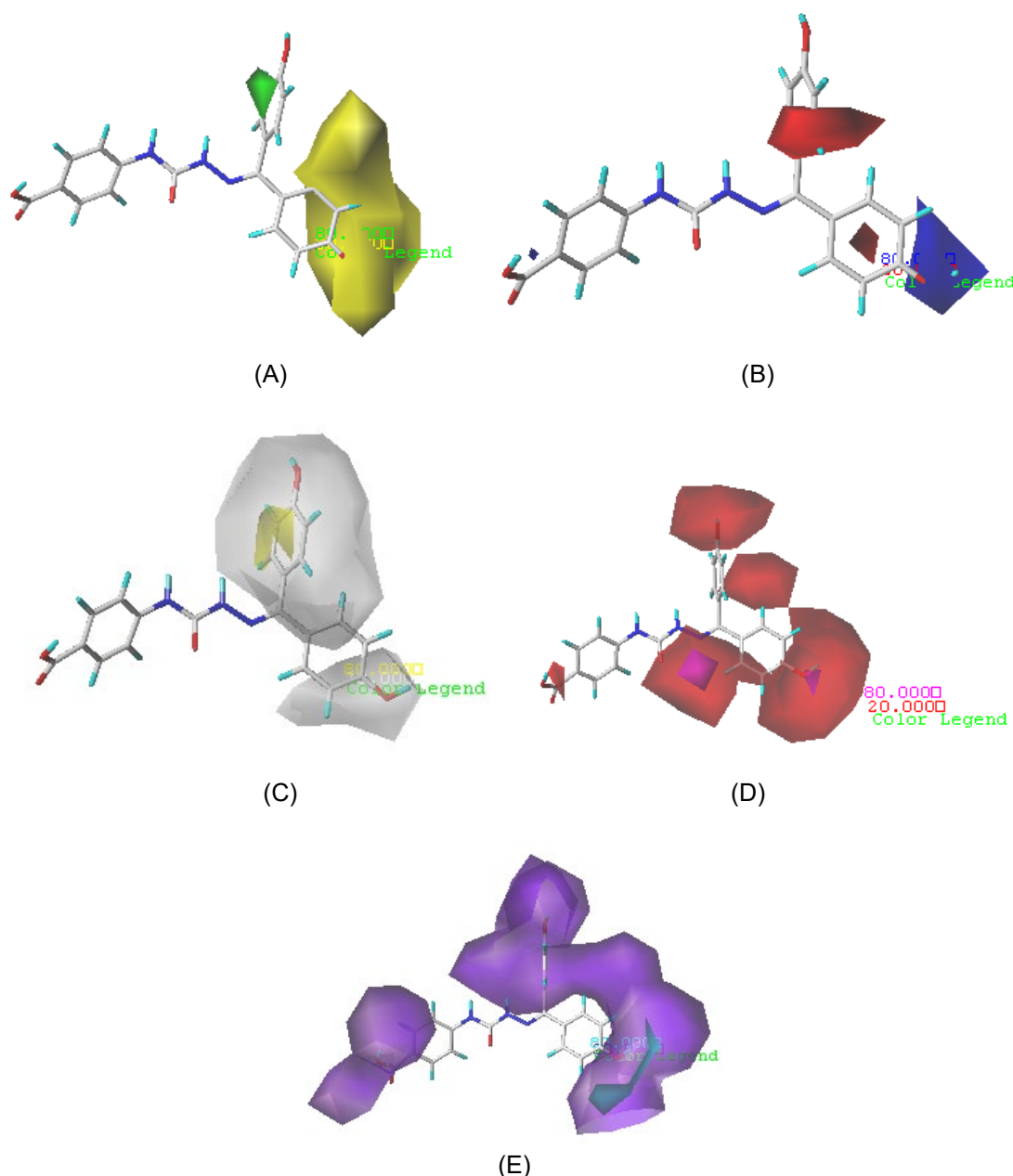

(A)   (B)

(C)   (D)

(E)

Figure 2. CoMSIA contour maps for compound 19. **A)** Steric fields. **B)** Electrostatic fields. **C)** Hydrophobic fields. **D)** H-bond acceptor fields. **E)** H-bond donor fields.

175

Orbital: Electron. J. Chem. 12 (4): 172-181, 2020

In H-bond donor field (Figure 2-E), the cyan region (20% contribution) indicates that introducing the H-bond group would be favorable for the potency, while purple color (20% contribution) disfavored hydrogen bond donors group. The purple contours map largely appeared around the phenyl ring of R1 and R2, which suggests that introducing H-bond donors substituents in the region could decrease the inhibitory activity, while a remarkable cyan contour could be observed at C4 position of R2, consequently, adding H-bond substituents at these positions will enhance compound activity.

These findings can be employed to guide the structure-based design of novel potential acetylcholinesterase inhibitors for further AD treatment.

2.3 Design for new molecules with AChE inhibitors activity

The information obtained from the contour maps not only provided deep insights into exploring the molecules features, but also helped to design new molecules with high inhibitory activities.

The SARs is summarized in Figure 3. According to the SARs revealed by the present work and related analysis results, new *p*-aminobenzoic acid derivatives were proposed and subjected to detailer analysis. The newly predicted activity values showed effective inhibition of Alzheimer than the most active compound 19 (pIC$_{50}$=7.337) for the generated models as depicted in Table 3.
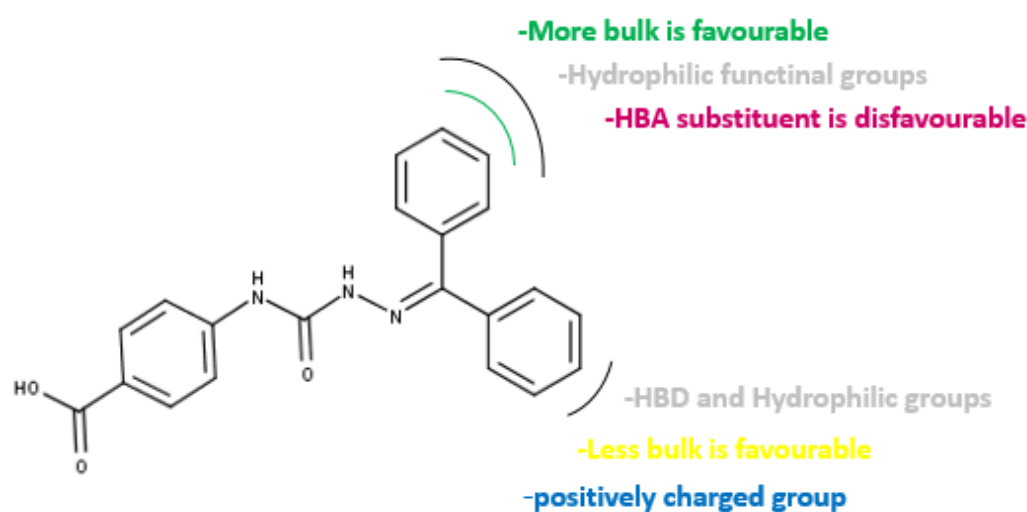

Figure 3. SAR summarized results from the QSAR study.
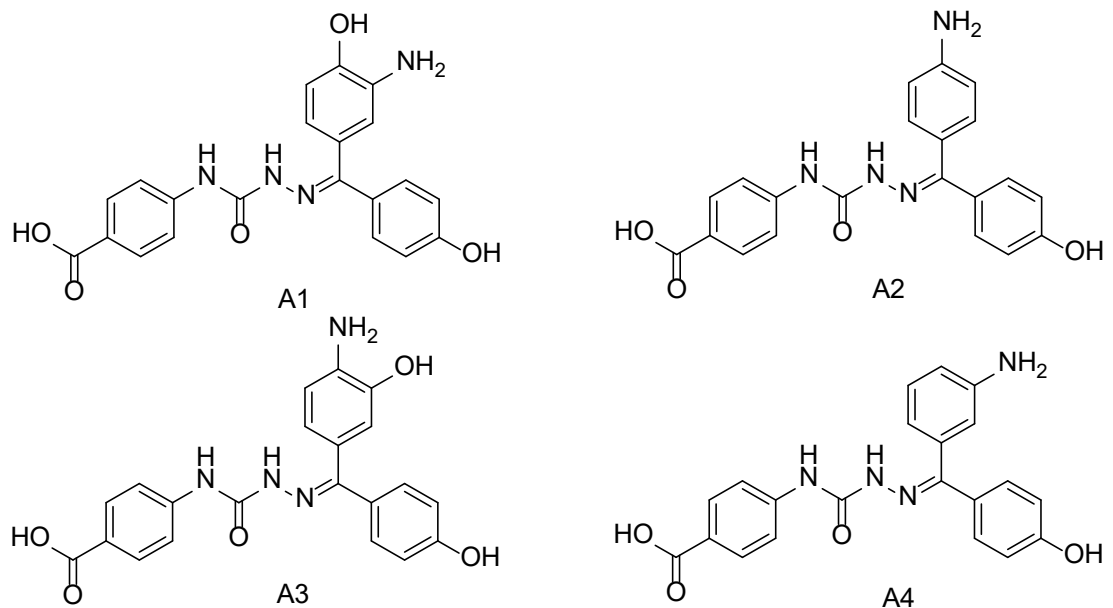
2.4 Docking results

Through molecular docking, we hope to gain deeper structural understanding of these inhibitors to AchE. Therefore, the most active compound 19 (figure 4) and the designed compound A1 (figure 5) were chosen for further docking analysis. They were molecularly docked with the X-ray crystallized complex of AchE receptor (PDB:1EVE) using Surflex-docking.

The docked pose of the designed compound A1 exhibited a higher total score of 7.0375 than that of the most active compound of the database (Compound 19, total score = 5.6842), forming 3 Hydrogen bond interactions of an oxygen atom from two hydroxyls and acid. Hydrogen bond interactions were formed from an interaction of amine with the active site residues TYR 70, ARG 289, HIS 440, and ARG 289. Furthermore, a pi–pi alkyl interaction was found between the phenyl ring attached to acid and the active residue PHE 330.

These interactions are the main factors having an important impact on the affinity of a ligand to the receptor, which match well with the results of hydrophobic and electrostatic contour maps, supporting the selected pose of the proposed compound A1 which could form a strong inhibitory effect on AchE.

176

Orbital: Electron. J. Chem. 12 (4): 172-181, 2020

Table 3. Newly proposed molecules and their predicted pIC$_{50}$.

	Predicted pIC$_{50}$	
N°	**CoMFA**	**CoMSIA**
A1	7.573	7.643
A2	7.543	7.595
A3	7.474	7.554
A4	7.437	7.499
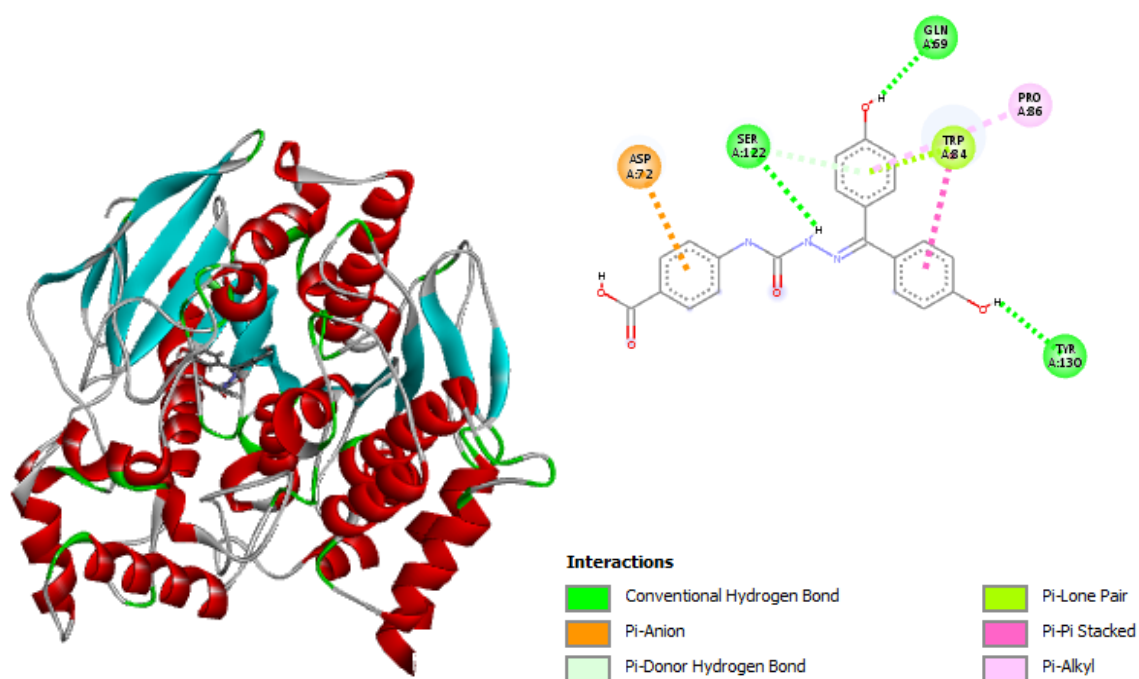
Figure 4. Docking interactions of compound 19 with AchE.

177

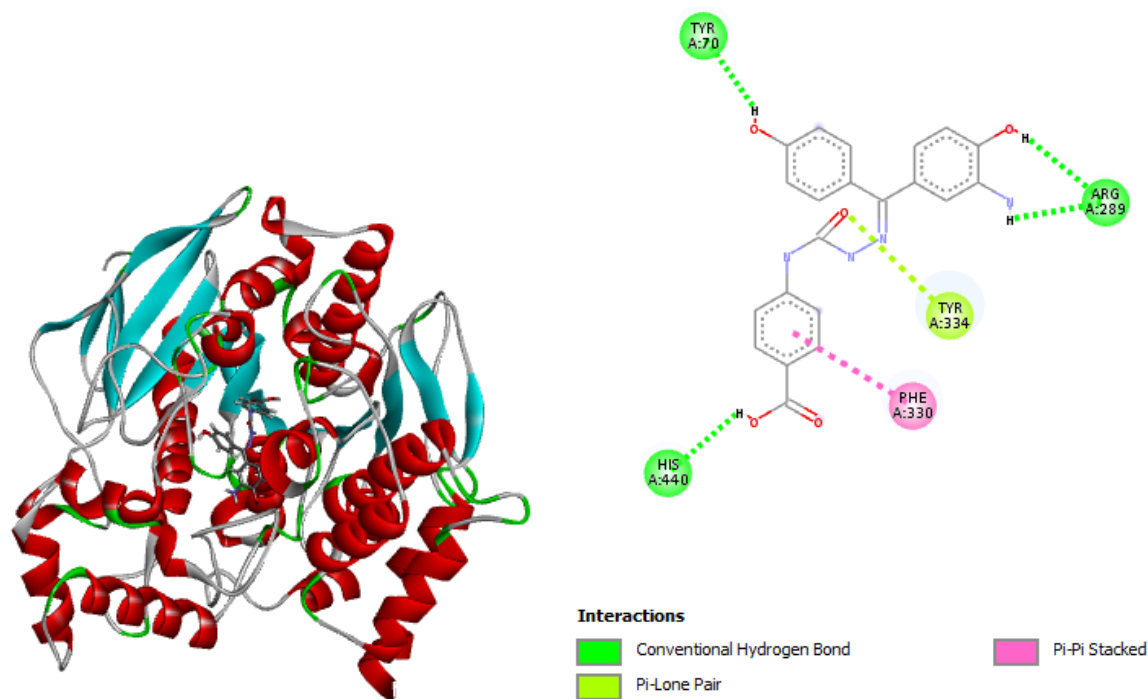*Orbital: Electron. J. Chem. 12 (4): 172-181, 2020*

Figure 5. Docking interactions of the proposed compound A1 with AchE.

2.5 Comparison with the references

For this class of acetylcholinesterase inhibitors, several *m-* and *p*-aminobenzoic acid derivatives have been synthesized [19, 20]. S. K. Shrivastava et al. [16] have designed and synthesized novel PABA derivatives and demonstrated that p-substituted derivatives, in comparison with *o-* and *m*-substituted derivatives, were more active. Through our SARs and molecular docking analyses, we have demonstrated that p-substituted derivatives were more active, which match well with the above demonstration. In addition, the newly designed compounds reported by the present work, in comparison with the previously synthesized PABA derivatives, have showed an important improvement in the inhibitory activity. So we firmly believe this is an important theoretical basis in designing novel PABA derivatives as potent inhibitors of acetylcholinesterase.

3. Material and Methods
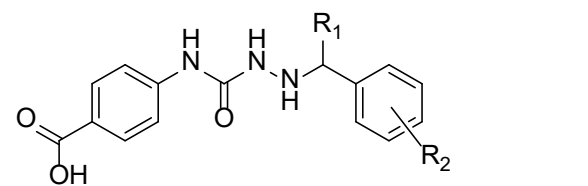
3.1 Data set

Based on a literature study, 20 *p*-aminobenzoic acid derivatives were selected and employed for molecular modeling [16]. Taking the structural diversity of biological data into consideration, the whole dataset was divided into a training set of 15 molecules in order to generate a robust model and a test of 5 molecules (superscript * in Table 4) to assess the reliability of the model. The acetylcholinesterase (AChE) inhibitor activities IC50 (μM) were converted into pIC_{50} values where pIC_{50} = −Log IC50, which were further used as dependent variables for QSAR analysis. The chemical structure of the molecules and their pIC_{50} values are available in Table 4.

3.2 Minimization and alignment

The 3D structures of all molecules were built and minimized using the SYBYL-X2.0 program [21]. The energy minimization processes of the studied molecules were performed using the SKETCH option in Sybyl program by Powell's conjugate gradient method under the Tripos standard force field [22], with Gasteiger-Hückel charges [23] and 0.01 kcal/mol Å as a convergence criterion.

The molecular alignment aims to enhance the linearity of the optimal QSAR models, the molecules were stratified on compound 19 by common substructure alignment using the simple alignment method in Sybyl [24] as shown in Figure 7.

178

Orbital: Electron. J. Chem. 12 (4): 172-181, 2020

Table 4. Chemical structure of PABA derivatives with AChE inhibitory activities.

N°	R₁	R₂	pIC50
1	H	H	4.372
2	H	2-OH	4.991
3	H	2,4-diOH	5.670
4	H	2,4,6-triOH	4.686
5	H	2-OCH3	4.188
6	H	2,4-diOCH3	4.049
7	H	2,4,6-triOCH3	3.941
8*	*H	4-OH-3,5-diOCH3	3.965
9*	CH3	H	6.900
10	CH3	4-OCH3	5.079
11	CH3	4-OH-3-OCH3	5.124
12	C2H5	H	5.327
13	C2H5	4-OCH3	4.544
14	C2H5	4-OH-3-OCH3	4.663
15	C6H5	H	7.301
16*	C6H5	4-OCH3	5.190
17*	C6H5	4-OCH3	4.801
18	4-OCH3C6H5	4-OH	7.301
19	C6H5	4-OH	7.337
20*	4-OC6H5	4,6-diOCH3	5.078

* Test set molecules

Figure 7. Core (above) and aligned compounds (below) using molecule 19 as a template.

3.3 3D-QSAR study

The molecular alignment is considered as the most important step in the generation of optimal models. Both CoMFA [25] and CoMSIA [26] were developed to improve the linearity between the obtained models and acetylcholinesterase inhibitory activities. During the 3D-QSAR study, the minimum sigma (column filtering) was limited to 2.0 kcal/mol, and 30 kcal/mol iterations was adopted as the energy cutoff values [27].

3.4 Statistical analysis and validation

The partial least squares (PLS) analysis was adopted to build the linear relationship between the biological activity and structure [28]. The PLS with leave-one-out cross-validation was carried out to calculate the optimum number of components (N) and the coefficient of cross-validation correlation (Q^2). The correlation coefficient (R^2), F-test value (F) and the standard error of estimate (SEE) were calculated by the non-cross validation procedure. Hence, the optimal resulting 3D-QSAR model is chosen based on high Q^2 and R^2 values ($Q^2 > 0.50$ and $R^2 > 0.60$), an optimal number of component values, and low standard error estimation (SEE). External validation was also employed to further evaluate the reliability of the generated models using five molecules as a test set. The best value of r_{ext}^2 should be more than 0.6 indicating good reliability of the generated 3D-QSAR model [29].

3.5 Molecular Docking

The molecular docking as a powerful approach, was conducted by the Surflex-Dock to gain a deeper understanding of the receptor-ligand structural interaction [30]. The generated results were analyzed using PyMol [31] and Discovery studio 2016 [32] software. Taking the total score into consideration, the best complex conformation was considered as the most satisfactory binding mode. The selected molecules were studied and the results of the 3D-QSAR model were compared.

3.5.1 Macromolecule preparation

The crystal structure 1EVE of AChE was imported from the Protein Data Bank. The Discovery Studio 2016 software was performed to prepare the protein by the addition of polar hydrogens and Kohlman charges and removing the co-crystallized ligand and all water molecules.

179

Orbital: Electron. J. Chem. 12 (4): 172-181, 2020

3.5.2 Ligand preparation

The 3D structures of the selected p-aminobenzoic Acid derivatives were geometrically optimized using the SKETCH option in SYBYL and energetically minimized using default parameters. And thus docked into the binding pocket of the AchE receptor.

4. Conclusions

In the current study, a combination of 3D-QSAR and molecular docking was used to explore the SARs for a series of selective p-aminobenzoic Acid derivatives as potent AChE inhibitors. The optimal models were validated internally and externally as demonstrated by the statistical criteria. The 3D-QSAR contour maps analysis helped to better interpret the feature requirements, revealing the crucial roles played by the electrostatic and hydrophobic substitutions to elevate the inhibitory potency. Several novel AchE inhibitors were designed in silico and the predicted activity was found to be higher than Compound 19 for the developed models. Additionally, the newly designed molecules were investigated for their interactions with AchE receptor using molecular docking. And consequently, hydrogen bonding and pi–pi alkyl interactions of several key residues (i.e., TYR 70, ARG 289, HIS 440 and PHE 330), were verified to be of importance for their ligand-receptor binding. Therefore, is demonstrated that the newly designed compounds have a reliable relationship between the electrostatic and hydrophobic effects and the AChE inhibitory potency justified by the obtained data. These findings provide valuable insights for the rational development of new AchE inhibitors with enhanced activity based on p-aminobenzoic Acid.

Acknowledgments

References and Notes

[1] Pradeepkiran, J.; Reddy, P. *Cells* **2019**, *8*, 260. [Crossref]

[2] Ustun, O.; Senol, F. S.; Kurkcuoglu, M.; Orhan, I. E.; Kartal, M.; Baser, K. H. C. *Ind Crops Prod* **2012**, *38*, 115. [Crossref]

[3] Scipioni, M.; Kay, G.; Megson, I. L.; Kong Thoo Lin, P. *MedChemComm* **2019**, *10*, 764. [Crossref]

[4] Karakaya, S.; Koca, M.; Yılmaz, S.; Yıldırım, K.; Pınar, N.; Demirci, B.; Brestic, M.; Sytar, O. *Molecules* **2019**, *24*, 722. [Crossref]

[5] Saeedi, M.; Mohtadi-Haghighi, D.; Mirfazli, S. S.; Mahdavi, M.; Hariri, R.; Lotfian, H.; Edraki, N.; Iraji, A.; Firuzi, O.; Akbarzadeh, T. *Chem. Biodivers.* **2019**, *16,* e1800433. [Crossref]

[6] Barai, P.; Raval, N.; Acharya, S.; Borisa, A.; Bhatt, H.; Acharya, N. *Behav. Brain Res.* **2019**, *356*, 18. [Crossref]

[7] Davies, P.; Maloney, J. F. *Lancet* **1976**, *308*, 1403. [Crossref]

[8] Iqbal, K.; Grundke-Iqbal, I. *Alzheimers Dement.* **2010**, *6*, 420. [Crossref]

[9] Robert, A.; Liu, Y.; Nguyen, M.; Meunier, B. *Acc. Chem. Res.* **2015**, *48*, 1332. [Crossref]

[10] Robert, A.; Liu, Y.; Nguyen, M.; Meunier, B. *Acc. Chem. Res.* **2015**, *48*, 1332. [Crossref]

[11] Tramutola, A.; Lanzillotta, C.; Perluigi, M.; Butterfield, D. A. *Brain Res. Bull.* **2017**, *133*, 88. [Crossref]

[12] Mattson, M. P.; Tomaselli, K. J.; Rydel, R. E. *Brain Res.* **1993**, *621*, 35. [Crossref]

[13] LaFerla, F. M.; Green, K. N.; Oddo, S. *Nature Rev. Neuro Sci.* **2008**, 499. [Crossref]

[14] Makhaeva, G. F.; Kovaleva, N. V.; Boltneva, N. P.; Lushchekina, S. V.; Rudakova, E. V.; Stupina, T. S.; Terentiev, A. A.; Serkov, I. V.; Proshin, A. N.; Radchenko, E. V.; Palyulin, V. A.; Bachurin, S. O.; Richardson, R. J. C. *Bioorganic Chem.* **2020**, *94*, 103387. [Crossref]

[15] Sivakumar, M.; Saravanan, K.; Saravanan, V.; Sugarthi, S.; kumar, S. M.; Alhaji Isa, M.; Rajakumar, P.; Aravindhan, S. *J. Biomol. Struct. Dyn.* **2020**, *38*, 1903. [Crossref]

[16] Shrivastava, S. K.; Sinha, S. K.; Srivastava, P.; Tripathi, P. N.; Sharma, P.; Tripathi, M. K.; Tripathi, A.; Choubey, P. K.; Waiker, D. K.; Aggarwal, L. M.; Dixit, M.; Kheruka, S. C.; Gambhir, S.; Shankar, S.; Srivastava, R. K. *Bioorganic Chem.* **2019**, *82*, 211. [Crossref]

[17] Tang, X.-M.; Hu, W.; Fan, L.; Wang, H.; Tang, M.-H.; Yang, D.-C. *Future Med. Chem.* **2020**, fmc-2018-0372. [Crossref]

[18] Krátký, M.; Konečná, K.; Janoušek, J.; Brablíková, M.; Janďourek, O.; Trejtnar, F.; Stolaříková, J.; Vinšová, J. 4 *Biomolecules* **2019**, *10*, 9. [Crossref]

[19] Correa-Basurto, J.; Alcántara, I. V.; Espinoza-Fonseca, L. M.; Trujillo-Ferrara, J. G. *Eur. J. Med. Chem.* **2005**, *40*, 732. [Crossref]

[20] Trujillo-Ferrara, J.; Montoya Cano, L.; Espinoza-Fonseca, M. *Bioorg. Med. Chem. Lett.* **2003**, *13*, 1825.

180

Orbital: Electron. J. Chem. 12 (4): 172-181, 2020

[Crossref]

[21] Tripos Inc., St. Louis, MO, USA, SYBYL-X 2.0, (n.d.). [Link]

[22] Clark, M.; Cramer, R. D.; Van Opdenbosch, N. *J. Comput. Chem.* **1989**, *10*, 982. [Crossref]

[23] Purcell, W. P.; Singer, J. A. *J. Chem. Eng. Data* **1967**, *12*, 235. [Crossref]

[24] AbdulHameed, M. D. M.; Hamza, A.; Liu, J.; Zhan, C.-G. *J. Chem. Inf. Model.* **2008**, *48*, 1760. [Crossref]

[25] Cramer, R. D.; Patterson, D. E.; Bunce, J. D. *J. Am. Chem. Soc.* **1988**, *110*, 5959. [Crossref]

[26] Klebe, G.; Abraham, U.; Mietzner, T. *J. Med. Chem.* **1994**, *37*, 4130. [Crossref]

[27] Ståhle, L.; Wold, S. 6 In: *Progress in Medicinal Chemistry*; Elsevier, **1988**; Vol. 25, pp 291. [Crossref]

[28] Bush, A. I. *J. Alzheimers Dis.* **2012**, *33*, S277. [Crossref]

[29] Baroni, M.; Clementi, S.; Cruciani, G.; Costantino, G.; Riganelli, D.; Oberrauch, E. *J. Chemom.* **1992**, *6*, 347. [Crossref]

[30] Sybyl 8.1; Tripos Inc.: St. Louis, MO, USA, 2008; Available online: http://www.tripos.com (accessed on 26 January 2011).

[31] DeLano, W. L. Pymol: An Open-Source Molecular Graphics Tool. *CCP4 Newsl. Protein Crystallogr.* **2002**, *40*, 82.

[32] Discovery Studio Predictive Science Application | Dassault Systèmes BIOVIA. https://www.3dsbiovia.com/products/collaborative-science/biovia-discovery-studio/ (accessed october, 2019.

181

Orbital: Electron. J. Chem. 12 (4): 172-181, 2020